Cellular and Molecular Bioengineering, Vol. 8, No. 3, September 2015 *(© 2015)* pp. 416–432
DOI: 10.1007/s12195-015-0389-4

Design of a Novel 3D Printed Bioactive Nanocomposite Scaffold for Improved Osteochondral Regeneration

NATHAN J. CASTRO,[1] ROMIL PATEL,[2] and LIJIE GRACE ZHANG[1,2,3]

[1]Department of Mechanical and Aerospace Engineering, The George Washington University, 800 22nd Street, NW, Washington, DC 20052, USA; [2]Department of Biomedical Engineering, The George Washington University, 800 22nd Street, NW, Washington, DC 20052, USA; and [3]Department of Medicine, The George Washington University, 800 22nd Street, NW, Washington, DC 20052, USA

(Received 6 February 2015; accepted 4 April 2015; published online 17 April 2015)

Associate Editor Christine Schmidt oversaw the review of this article.

Abstract—Chronic and acute osteochondral defects as a result of osteoarthritis and trauma present a common and serious clinical problem due to the tissue's inherent complexity and poor regenerative capacity. In addition, cells within the osteochondral tissue are in intimate contact with a 3D nanostructured extracellular matrix composed of numerous bioactive organic and inorganic components. As an emerging manufacturing technique, 3D printing offers great precision and control over the microarchitecture, shape, and composition of tissue scaffolds. Therefore, the objective of this study is to develop a biomimetic 3D printed nanocomposite scaffold with integrated differentiation cues for improved osteochondral tissue regeneration. Through the combination of novel nano-inks composed of organic and inorganic bioactive factors and advanced 3D printing, we have successfully fabricated a series of novel constructs which closely mimic the native 3D extracellular environment with hierarchical nanoroughness, microstructure, and spatiotemporal bioactive cues. Our results illustrate several key characteristics of the 3D printed nanocomposite scaffold to include improved mechanical properties as well as excellent cytocompatibility for enhanced human bone marrow-derived mesenchymal stem cell adhesion, proliferation, and osteochondral differentiation *in vitro*. The present work further illustrates the effectiveness of the scaffolds developed here as a promising and highly tunable platform for osteochondral tissue regeneration.

Keywords—3D printing, Nanocomposite, Osteochondral, Stem cell, Bioactive, Biomimetic, Growth factor delivery.

INTRODUCTION

Osteochondral defects, caused by osteoarthritis (OA) and trauma, present a common and serious clinical problem. In particular, OA is a leading cause of disability in the United States which manifests clinically as degeneration of the articular surface in synovial joints leading to compromised structural integrity of the joint. When articular cartilage within the knee joint progressively wears away, the protective surface between the femur and tibia is compromised

Address correspondence to Lijie Grace Zhang, Department of Mechanical and Aerospace Engineering, The George Washington University, 800 22nd Street, NW, Washington, DC 20052, USA. Electronic mail: lgzhang@gwu.edu

This article is part of the 2015 Young Innovators Issue.

Lijie Grace Zhang is an assistant professor in the Department of Mechanical and Aerospace Engineering, Department of Biomedical Engineering and Department of Medicine at the George Washington University. She obtained her Ph.D. in Biomedical Engineering at Brown University in 2009. Dr. Zhang joined GW in 2010, after finishing her postdoctoral training at Rice University and Harvard Medical School. Currently she directs the Bioengineering Laboratory for Nanomedicine and Tissue Engineering at GW. She has received the NIH Director's New Innovator Award, GW SEAS Outstanding Young Researcher Award, John Haddad Young Investigator Award by American Society for Bone and Mineral Research, the Early Career Award from the International Journal of Nanomedicine, Ralph E. Powe Junior Faculty Enhancement Award by the Oak Ridge Associated Universities Organization, Joukowsky Family Foundation Outstanding Dissertation Award at Brown and the Sigma Xi Award. Her research interests include nanomaterials, 3D bioprinting, complex tissue engineering, stem cell engineering, drug delivery and breast cancer bone metastasis. Dr. Zhang has authored 2 books, over 60 journal papers, book chapters and conference proceedings, 3 patents and has presented her work on over 150 conferences, university and institutes.

leading to painful bone-on-bone contact resulting in impinged movement. Millions of Americans suffer from symptoms including: bone spurs, joint discomfort, chronic pain, and loss of movement due to degenerative loss of cartilage tissue.[7] Currently, OA affects 48 million Americans and is projected to affect 67 million Americans by 2030.[23] Although OA is of pressing national concern, current treatment methods are limited or inefficient combinations of pharmacologic and invasive surgical procedures.[4] Specifically, many joint defects are addressed through the use of autografts, allografts, mosaicplasties, microfracture surgery as well as combinations thereof[16,41,54] with many issues related to insufficient donor tissue, donor site morbidity, inadequate host tissue integration, surface incongruency, *etc*. Therefore, better strategies are necessary for the treatment of OA.

Tissue engineering (TE) has emerged as an interdisciplinary field with great potential to develop novel therapeutic approaches for OA and degenerative joint disease. Concepts of TE treatment offer the advantage of combining viable autologous or transplanted cells, growth factors, and scaffolds for osteochondral defect repair.[10,56] The osteochondral (bone–cartilage) interface plays a critical role as the site of attachment between hyaline articular cartilage and subchondral bone. In addition, it provides the mechanical structure to support energy transfer of biomechanical movements. Unfortunately, damaged osteochondral tissue is difficult to treat due to the poor regenerative capacity of hyaline cartilage and the presence of complex biological and chemical gradients from the articulating surface to the underlying subchondral bone. As a result, interfacial tissue engineering has emerged as a subspecialty in TE focused on overcoming challenges of connecting various disparate tissue types in an effort to better match physiological, biomechanical, and biochemical signaling properties. Therefore, it is imperative to design and manufacture TE scaffolds with great precision over the following characteristics: appropriate biocompatible and mechanical properties, biodegradability, 3D biomimetic architecture, and bioactivity.[22,25,26,38]

Several advanced fabrication techniques have been utilized for the manufacture of 3D osteochondral scaffolds to include the extension of additive manufacturing technologies such as stereolithography (SL),[3] fused deposition modeling (FDM),[6,21,46,51] inkjet bioprinting,[33] and selective laser sintering (SLS).[12,14] These 3D printing technologies illustrate great promise in designing and controlling the overall scaffold structure while allowing for the incorporation of bioactive factors rendering the fabricated scaffolds more biomimetic and highly flexible in design. In addition, reproducible and highly-organized microarchitecture with patient-specific geometry through precise control over scaffold porosity, pore size, and interconnectivity has shown to greatly influence cellular behavior and modulate resultant tissue formation.[34,43,44,48] However, clinical applicability of rapid prototyped biodegradable constructs for orthopedic TE applications has been limited due to a dearth of available materials with suitable physical and biological properties. Furthermore, human osteochondral tissue is nano in the smallest dimension; however, current technologies for 3D bioprinting scaffolds with nanoscale features are limited.

Therefore, the work presented here aims to address current 3D printing limitations through the development of a novel FDM based investment casting system integrated with nanobiomaterials for the fabrication of biomimetic biphasic osteochondral scaffolds. The current system serves to utilize several advantages of rapid prototyping as well as explore the use of biomimetic nanobiomaterials within a biocompatible hydrogel-based matrix for tissue-specific modulation of human bone marrow-derived mesenchymal stem cells (hMSCs). Miller *et al*.[39] employed a similar printing technique to fabricate perfusable vascular networks within a hydrogel-based network through the use of a carbohydrate-based ''sugar glass''. Unlike the previous work, the system developed herein not only utilizes commercially available printing materials and biocompatible hydrogels, but also biomimetic and bioactive nanobiomaterials. Therefore, the extension of nanobiomaterials for 3D printing and subsequent evaluation of novel biphasic nanocomposite scaffolds is highly desirable for tissue and organ regeneration. Moreover, the current approach yields a highly interconnected and porous microstructured scaffold effectively addressing limitations specific to nutrient transportation and cell infiltration. In addition, the technique developed here greatly extends the capacity of commercially available 3D printing technology and green chemistry by eliminating the need of harsh printing conditions and unfavorable solvents.

In summary, with the use of computer-aided drafting (CAD) software and table-top FDM printing, we have efficiently produced highly porous interconnected scaffolds with mechanical properties conducive to osteochondral tissue regeneration. In addition, the effectiveness of incorporating biological cues for sustained delivery and directed hMSC chondrogenic and osteogenic differentiation was explored. Biphasic biomimetic scaffolds were fabricated containing near physiological concentrations of hydrothermally treated nanocrystalline hydroxyapatite (nHA, nanoscale bone minerals found in calcified cartilage and subchondral bone of osteochondral tissue) within the highly porous subchondral bone layer and chondrogenic transform-

ing growth factor-β1 (TGF-β1) in the cartilage layer for enhanced osteochondral regeneration. The current work illustrates the effectiveness of investment casting in fabricating physiologically relevant nanocomposite scaffolds for directed hMSCs function *in vitro*.

MATERIALS AND METHODS

3D Printing Biphasic Osteochondral Scaffolds

Synthesis of Biomimetic Hydrothermally Treated nHA

A well-established wet chemistry and hydrothermal treatment method was employed to synthesize nHA with nanometer size and crystallinity. In brief, 37.5 mL of a 0.6 M ammonium phosphate (Sigma Aldrich, St. Louis, MO) solution was added to 375 mL of water and adjusted to a pH of 10 with ammonium hydroxide (Fisher Scientific, Pittsburgh, PA). Subsequently, 1 M calcium nitrate (Sigma Aldrich, St. Louis, MO) was titrated into the above mixture at a rate of 5 mL/min while stirring. Precipitation of amorphous HA proceeded for 10 min at room temperature. The mixture containing HA precipitate was hydrothermally treated at 200 °C for 20 h in a 125 ml Teflon liner (Parr Instrument Company, Moline, IL). After 20 h, the nHA precipitate was centrifuged and rinsed thoroughly with water three times, dried at 80 °C for 12 h and ground into a fine powder and thoroughly characterized as described in our previous work.[27,50,55,59,62,65]

3D Biphasic Scaffold Design, Printing, and Fabrication

A 35 mm × 35 mm × 5 mm biphasic high impact polystyrene (HIPS) mold was designed in Rhinoceros 3D (McNeel North America, Seattle, WA). The CAD file was converted to a computer numerical control file with pre-configured in-fill density and *x*-, *y*-, *z*-axis tool head position then printed via a table-top FDM printer (Solidoodle©, Brooklyn, NY). The 5 mm biphasic mold was composed of a 3.8 mm (40% in-fill density) osseous layer and a 1.2 mm (0% in-fill density) cartilage layer. Upon printing of the biphasic mold, a biocompatible photocrosslinkable hydrogel solution composed of poly(ethylene glycol)-diacrylate (PEG-DA, Mn = 700): poly(ethylene glycol) (PEG, MW = 300) (60% wt/wt) was prepared and used as the bulk matrix material for all fabricated scaffolds. Photocrosslinking was expedited through the addition of the photoinitiator bis(2,4,6-trimethylbenzoyl)-phenylphosphineoxide (BAPO) donated by Ciba Specialty Chemicals (Tarrytown, NY), with excitation (355 nm)in the ultraviolet (UV) range at a concentration of 0.5 wt% of PEG-DA. BAPO was selected for its excellent solubility in PEG eliminating the need of harsh organic solvents or surfactants. A flow chart illustrating the scaffold design and fabrication process is shown in Fig. 1. A series of scaffolds were fabricated with nHA concentrations ranging from 0 to 60% (wt/wt of PEG-DA) for the osseous layer and bare PEG-DA:PEG was subsequently cast as the solid cartilage layer. In an effort to render the scaffold more applicable to osteochondral tissue regeneration, 10 ng/mL TGF-β1 was incorporated into the uncured cartilage layer of the biphasic scaffold. The cast 3D printed HIPS molds were UV cured for 4 min from above and inverted and UV cured for an additional 4 min.

Crosslinked samples were ultrasonicated in a 33.0 vol% solution of D-limonene (Amazon, Seattle, Washington) in 100 g-scale reaction conditions for two 90-min periods at 40 °C followed by two 90-min washes in distilled water at 40 °C to remove any residual HIPS and allow for swelling and dissolution of the soluble PEG fraction. D-Limonene is an environmentally friendly solvent which readily dissolves HIPS and has no adverse reaction to crosslinked PEG thus eliminating the use of halogenated solvents traditionally used in the dissolution of polymeric materials. Upon completion, a 5 mm biopsy punch was used to collect cylindrical samples. A 3D rendering of the fabricated scaffold with highlighted microchannel structure is shown in Fig. 2. FDM printing parameters with corresponding scaffold microarchitectural effects are shown in Table 1. Briefly, the microchannel pore size can be adjusted by altering the nozzle diameter of the extruding head as well as modifying the extrusion multiplier within the Slic3r software package. A nozzle diameter of 325 μm with an extrusion multiplier of 0.6 yielded a printed filament of ~240–270 μm resulting in a pore diameter of equivalent dimension. In addition, pore density of the fabricated scaffold can be controlled by altering the in-fill density of the polymer mold. An in-fill density of 40% was used and resulted in a 40% porous structure in the osseous layer of the biphasic scaffold as seen in Fig. 2.

3D Printed Osteochondral Scaffold Characterization

Optical and Scanning Electron Microscopy (SEM)

For optical microscopy, scaffolds in the absence of nHA and growth factors were allowed to air dry overnight and imaged via a CM4210 optical system with manual zoom (×6.4) and fine focus (656 × 492 pixel size) (DSA25, Krüss USA, Matthews, NC). Similarly, for SEM analysis (Zeiss NVision 40 FIB, Thornwood, NY) samples containing 0–60 wt% nHA in the osseous layer were allowed to dry overnight at

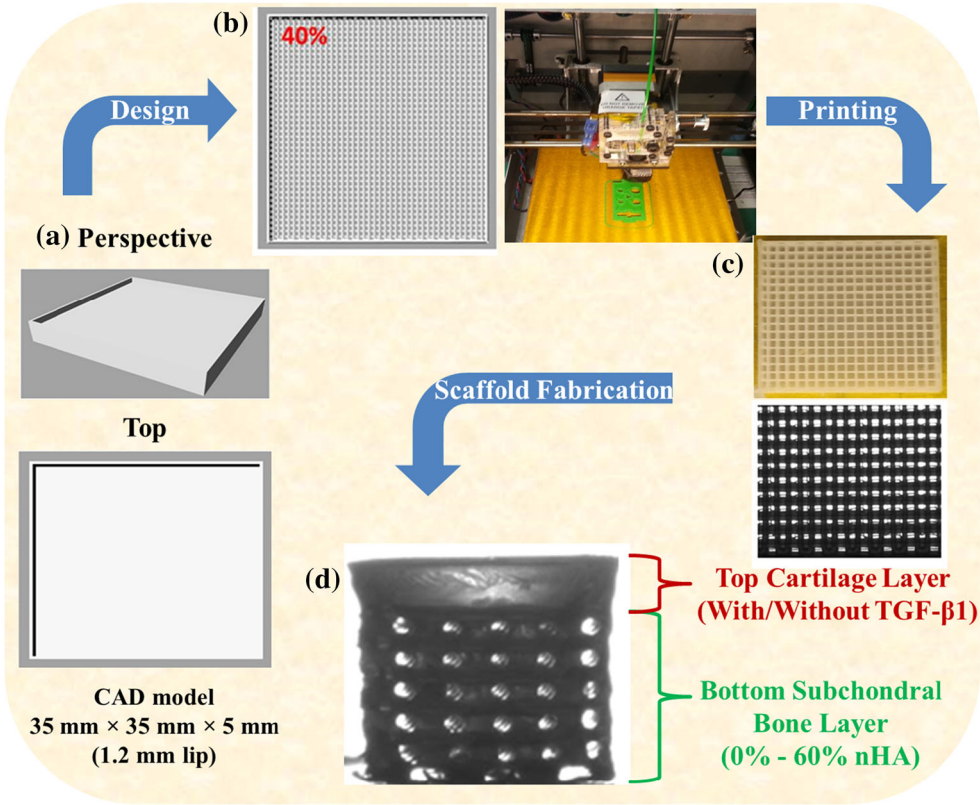

FIGURE 1. A flow chart of 3D printing novel osteochondral nanocomposite scaffold. (a) Computer-aided design (CAD) model of biphasic mold, (b) tool path for FDM print head and the photo image of the 3D printer, (c) optical micrograph of 3D printed HIPS mold, and (d) the final PEG-DA biphasic hydrogel scaffold.

room temperature prior to viewing at 3 kV accelerating voltage.

Mechanical Testing

The compressive modulus of the 3D printed scaffolds with and without nHA was determined via uniform compression testing (n = 5, Applied Test Systems, Butler, PA) fitted with a 100 N load cell at a crosshead speed of 5 mm/min. 5 mm samples were placed in ultrapure water and allowed to swell for 24 h with intermittent exchange of fresh ultrapure water and blotted dry prior to testing.

Bioactive Protein Release Study

In order to characterize the capacity of our 3D printed scaffold for sustained bioactive factor delivery, a model bioactive protein–bovine serum albumin (BSA), was utilized to characterize the rate of release and evaluated in two osteochondral scaffolds with and without nHA. BSA is a commonly used model protein to effectively characterize polymer-based sustained delivery systems.[1,35,57] Briefly, scaffolds containing 1 mg/mL BSA in the cartilage layer and 60% nHA in the bone layer were fabricated according to the previously described procedure. 5 mm samples (n = 5) were incubated in phosphate-buffered saline (PBS) at 37 °C. Fractions of the supernatant were centrifuged and collected at 4, 8, 24, and 48 h and 3, 5, 7, 14, and 21 days, respectively. The released BSA content was measured spectrophotometrically (Multiskan GO® Spectrophotometer, Thermo Scientific, Waltham, MA). Cumulative protein release profiles were plotted as a fraction of total encapsulated protein where total protein was determined by expedited digestion of samples of known mass in 10 M NaOH and absorbance measured at 280 nm.

hMSC Adhesion, Growth and Osteochondral Differentiation Behavior in the Novel Osteochondral Scaffolds In Vitro

Cell Culture

Primary MSCs were obtained from healthy consenting donor's iliac crest (female; age: 27) harvested at Tulane University under an IRB-approved protocol with informed consent and purchased from the Texas A&M Health Science Center, Institute for Regen-

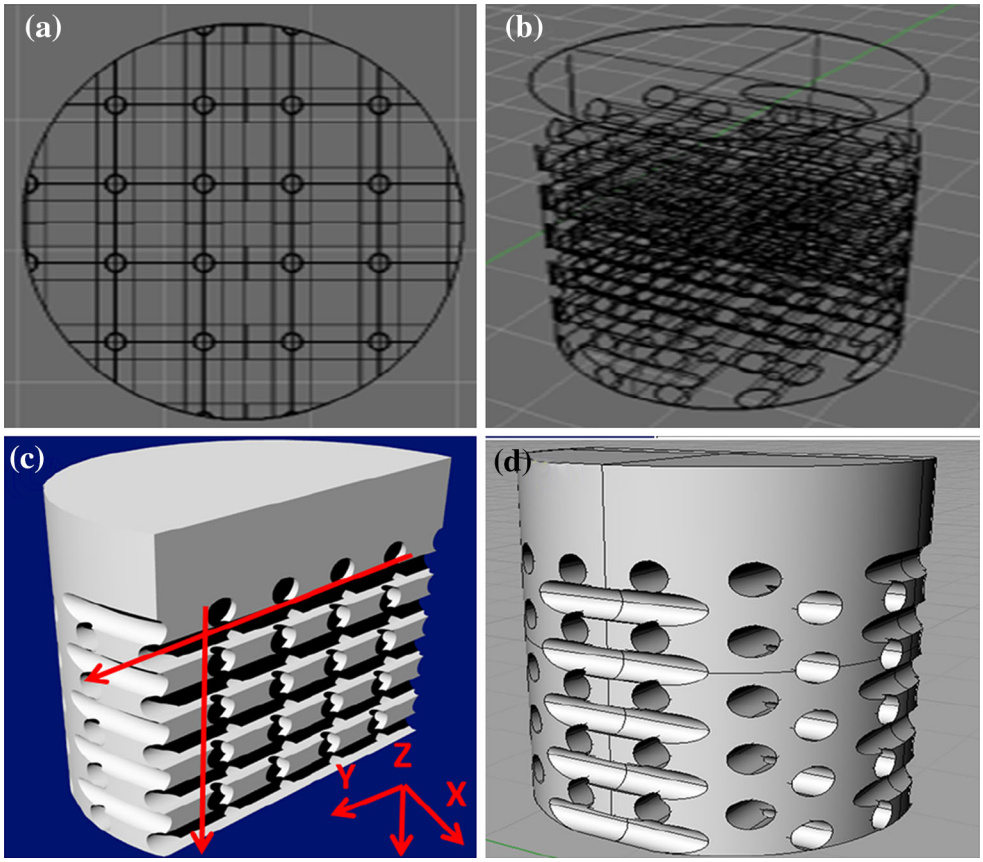

FIGURE 2. 3D rendering of biphasic osteochondral scaffolds (a top, b and d side, and c cross-sectional views). Arrows illustrate direction of internal microchannels.

TABLE 1. Correlation of FDM printing parameters and scaffold structure.

FDM printing for hydrogel investment casting	
FDM printing parameter	Corresponding scaffold feature
Nozzle diameter (325 μm)Extrusion multiplier (0.6)	Pore diameter (240–270 μm)
In-fill density (40%)	Pore density (40%)
In-fill pattern (rectilinear)	Internal microchannel architecture (orthogonal channel structure)

erative Medicine. We had the fully executed Material Transfer Agreement needed to obtain the cells. hMSCs (passage #3–6) were cultured in complete media composed of Alpha Minimum Essential medium (α-MEM, Gibco, Grand Island, NY) supplemented with 16.5% fetal bovine serum (FBS, Atlanta Biologicals, Lawrenceville, GA), 1% (v/v) L-glutamine (Invitrogen, Carlsbad, CA), and 1% penicillin:streptomycin (Invitrogen, Carlsbad, CA) and cultured under standard cell culture conditions (37 °C, a humidified, 5% CO_2/95% air environment).

hMSC Adhesion and Proliferation Study

Biphasic scaffolds containing 0–60 wt% nHA were studied in an effort to optimize nHA concentration. All 3D printed scaffolds were sterilized in 70% ethanol for 30 min then washed three times in PBS before cell seeding. hMSCs were seeded at a density of 50,000 cells/scaffold. Seeded scaffolds were then incubated under standard cell culture conditions for 4 h. After rinsing with PBS, the adherent cells were lifted enzymatically with 0.25% Trypsin–EDTA (Sigma Aldrich, St. Louis, MO) and quantified via a CellTiter 96® AQueous Non-Radioactive Cell Proliferation Assay (MTS assay, Promega, Madison, WI) and analyzed at 490 nm. Similarly, hMSC proliferation was examined on biphasic scaffolds with nHA concentrations of 0, 40, and 60 wt% of PEG-DA. hMSCs were seeded at a density of 10,000 cells/scaffold and incubated for 1, 3, and 5 days under standard cell culture conditions.

After rinsing with PBS, the adherent cells were quantified as previously described.

hMSC Chondrogenic and Osteogenic Differentiation Studies

hMSCs were seeded at a density of 10^5 cells/scaffold for chondrogenic and osteogenic differentiation studies. A bare (TGF-β1− and nHA−) biphasic scaffold (cartilage layer/bone layer) served as a control alongside the following experimental groups (TGF-β1− and nHA+) and (TGF-β1+ and nHA+). 60% nHA was selected based on hMSC adhesion and proliferation results. Cell seeded biphasic scaffolds were cultured in standard MSC complete media without supplementation of differentiation factors for 1, 2, and 3 weeks, respectively. At each prescribed time point, cell seeded samples were rinsed with PBS, lyophilized, then digested in a papain digestion solution for 18 h at 60 °C and stored at −80 °C until analyzed.

Glycosaminoglycan (GAG), a key component of cartilage matrix, was measured using a standard GAG assay kit (Accurate Chemical & Scientific Corp., Westbury, NY) similar to our previous studies.[9,19,20] Specifically, a predetermined volume of sample and buffer solution was added to a microcentrifuge tube with 500 μL of dye reagent and mixed for 30 min. The GAG–dye complex was centrifuged for 10 min at 10,000×g until a pellet was visible. The supernatant was decanted and all residual fluid was blotted dry. Next, 600 μL of dissociation reagent was added to the tubes and shaken for 30 min; 100 μL of each solution was placed into a 96-well plate and analyzed in triplicate. Absorbance was read at 656 nm and correlated to a standard curve of known standards.

Human type I and type II collagen were evaluated via type I and type II collagen enzyme-linked immunosorbent assay (ELISA) (Fisher Scientific, Pittsburgh, PA) per manufacturer's instruction. Briefly, digested control and sample aliquots were added to pre-coated 96-well plates with rat immunoglobulin M and immunoglobulin G capture antibodies, respectively and incubated at room temperature for 2 h. Unbound sample was washed and collagen type I/II specific detection antibodies were added and incubated for an additional 2 h and washed. After washing, streptavidin peroxidase (type I) or tetramethylbenzidine (type II) was added producing a color change. The reaction was stopped by the addition of an acidic stop solution and read at 490 nm (type I) and 450 nm (type II), respectively.

Calcium deposition, one of the most important indicators of osteogenic differentiation, was measured using a calcium reagent kit (Pointe Scientific Inc.). Specifically, after hMSC lysis, the scaffolds containing deposited calcium were immersed in a 0.6 N HCl solution at 37 °C for 24 h. After the prescribed time period, the amount of dissolved calcium present in the acidic supernatant was measured by reacting with the *o*-cresolphthalein complexone to form a purple tinted solution. Absorbance was measured by a spectrophotometer at 570 nm. Total calcium deposition was calculated from standard curves of known calcium concentrations run in parallel with experimental groups.

Total collagen content of lysed samples was evaluated via Sircol collagen assay kit (Accurate Chemical & Scientific Corp., Westbury, NY). Per manufacturer instructions, 1 mL dye reagent was added to 100 μL lysate and shaken for 30 min. Samples were then centrifuged for 10 min at 10,000 rpm to pellet the collagen-dye complex and the supernatant was carefully decanted. Ice-cold wash reagent was used to remove unbound dye and the samples were centrifuged once more and the supernatant decanted. A 250 μL alkali solution was added to solubilize the pellet and a 200 μL aliquot was transferred to a new 96-well plate and absorbance measurements were taken at 555 nm.

Statistical Analysis

Data are presented as the mean value ± standard error of the mean and Student's t test was used to determine differences amongst the groups. Statistical significance was considered at $p < 0.05$.

RESULTS

3D Printed Biphasic Nanocomposite Osteochondral Scaffolds

Optical and SEM images (Fig. 3) of fabricated osteochondral scaffolds revealed excellent horizontal and vertical pore formation with smooth integration between the cartilage and subchondral bone layer. Figures 3a–3c illustrates the gross morphology of the fabricated 3D biphasic osteochondral scaffolds. SEM images of the fabricated scaffold (Figs. 3d–3f) illustrate highly ordered and uniform pore size and spacing with pore sizes ranging from 225 to 260 μm. Due to the casting, bulk crosslinking, and mold dissolution manufacturing technique employed here a very smooth transition between the respective layers was formed. In addition, SEM analysis (Fig. 4) showed nanoscale surface morphological changes of 3D printed scaffolds containing different concentrations of nHA when compared to controls. More nHA particles were noticeable on scaffolds containing higher concentrations of nHA.

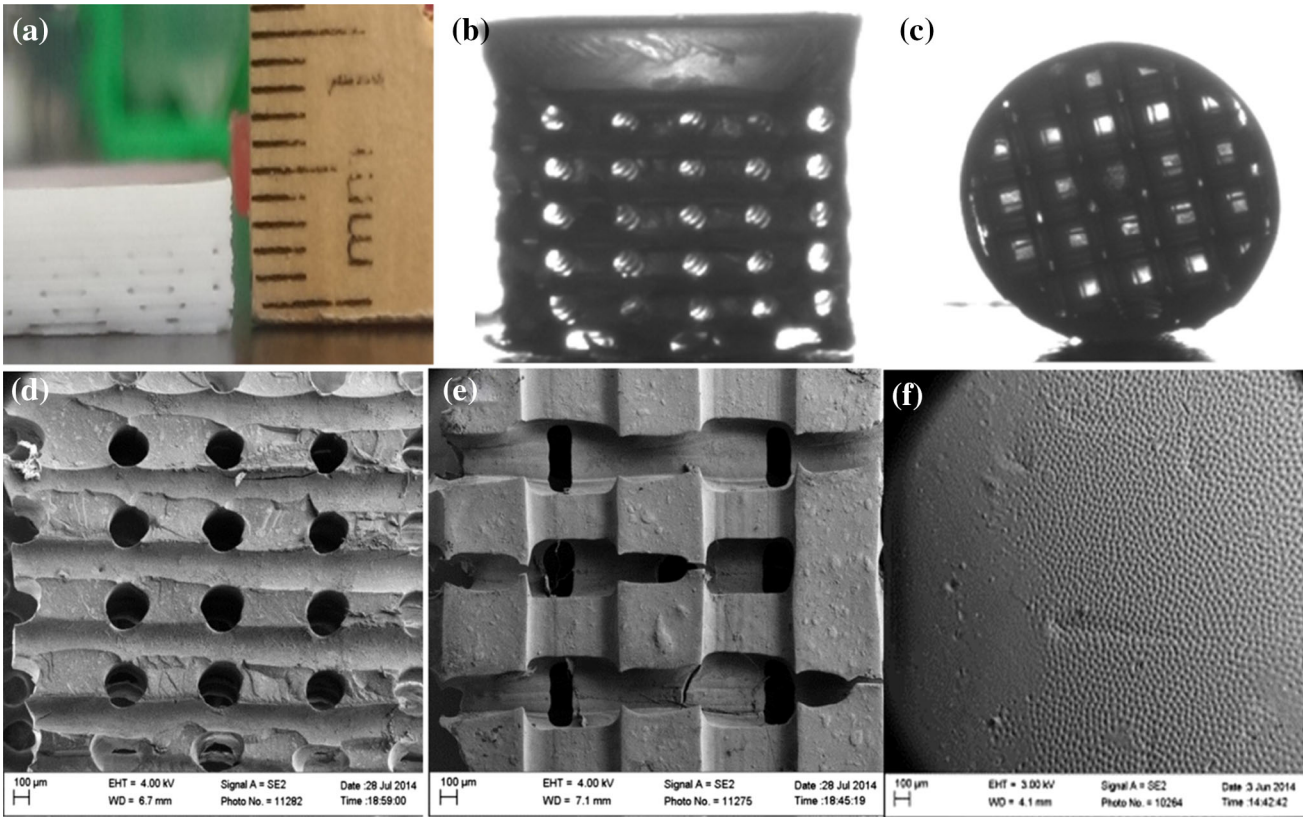

FIGURE 3. Our novel biphasic osteochondral scaffold. (a) A photo image of the fabricated biphasic hydrogel scaffold sheet (cross-sectional view) before puncture. Optical micrograph of cylindrical biphasic osteochondral scaffold (b) side view and (c) top view illustrating horizontal and vertical channels. (d–f) SEM images of different regions of the biphasic osteochondral scaffold.

The presence of nHA nanoparticles within the porous bone layer yields a more biomimetic scaffold with respect to nanoscale morphology and bioactivity as well as aids in enhancing the compressive strength of the overall scaffold (Fig. 5). Similar to our previous studies, morphological analysis of synthesized nHA displayed grain sizes in the range of 50–100 nm in length and 20–30 nm in width.[27] More importantly, with the incorporation of 60 wt% nHA in the subchondral region, a 61% increase in compressive modulus and 87% increase in ultimate compressive strength were observed.

BSA release studies were conducted as well to determine bioactive factor release kinetics of the nanocomposite osteochondral scaffold system developed here. Figure 6 shows the cumulative release profiles of biphasic scaffolds with and without the presence of 60 wt% nHA. An interesting phenomenon was observed with regards to nHA-containing scaffolds where the nanocomposite scaffolds exhibited greatly decreased initial burst release when compared to pure hydrogel samples with ~45% total protein released after 1 week of incubation and sustained delivery over 21 days.

Enhanced hMSC Adhesion and Growth in the Novel Biphasic Nanocomposite Osteochondral Scaffolds

Figure 7 displays the 4-h hMSC adhesion study on fabricated scaffolds containing nHA concentrations ranging from 0 to 60 wt%. The results illustrated a linear correlation between hMSC adhesion and nHA concentration. More importantly, the scaffolds containing near physiological concentration (40 and 60 wt%) exhibited the greatest increase in cell density of 108 and 114%, respectively, thus suggesting the excellent cytocompatibility of the fabricated nanocomposite scaffolds. Notwithstanding, lower nHA concentrations also showed an increase in cell density of 28, 67, and 88% for 5, 10, and 20 wt% nHA samples, respectively, serving to illustrate the effectiveness of nHA in increasing cell adhesion even at low concentrations.

Based on the results of the hMSC adhesion study, a 5-day proliferation study was performed amongst 40

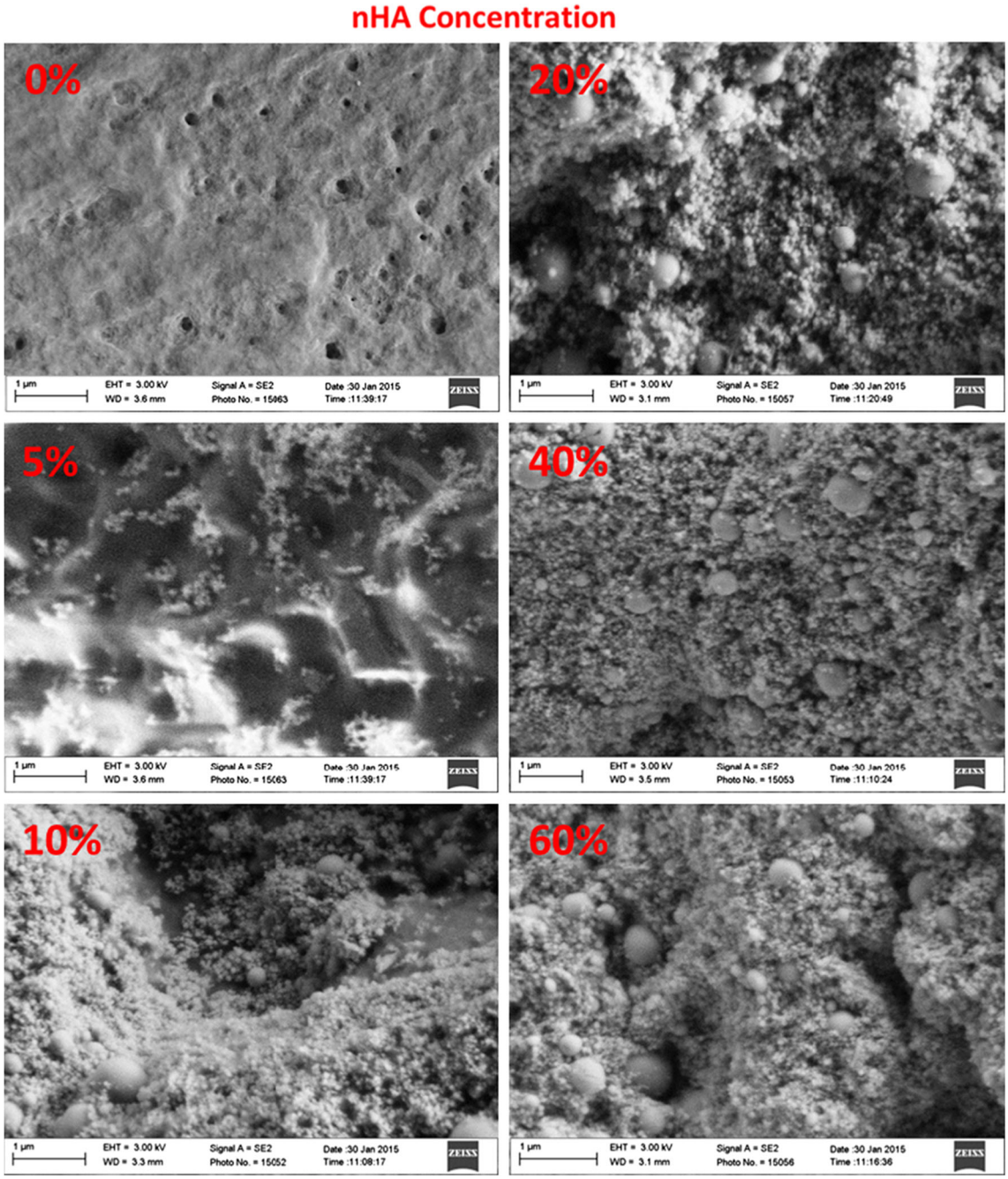

FIGURE 4. SEM images of different concentration of nHA distribution (0, 5, 10, 20, 40 and 60 wt%) within our 3D printed osteochondral scaffolds at high magnification. All nHA sample groups showed increased surface roughness with increased nHA concentration when compared to control.

and 60 wt% sample groups (Fig. 8). Similarly, when compared to non-nHA-containing scaffolds, hMSC proliferation was enhanced with the incorporation of biomimetic nHA particles. After 1 day of culture, 40 and 60 wt% nHA samples groups exhibited an increase in hMSC proliferation of 93 and 53% over control. This trend continued after 5 days of culture with a 43 and 57% increase over control.

Greatly Improved hMSC Chondrogenic and Osteogenic Differentiation in the Novel Biphasic Osteochondral Scaffolds Containing Osteogenic nHA and Chondrogenic TGF-β1

For hMSC osteochondral differentiation studies, the biphasic osteochondral scaffold was evaluated for chondrogenic and osteogenic differentiation potential,

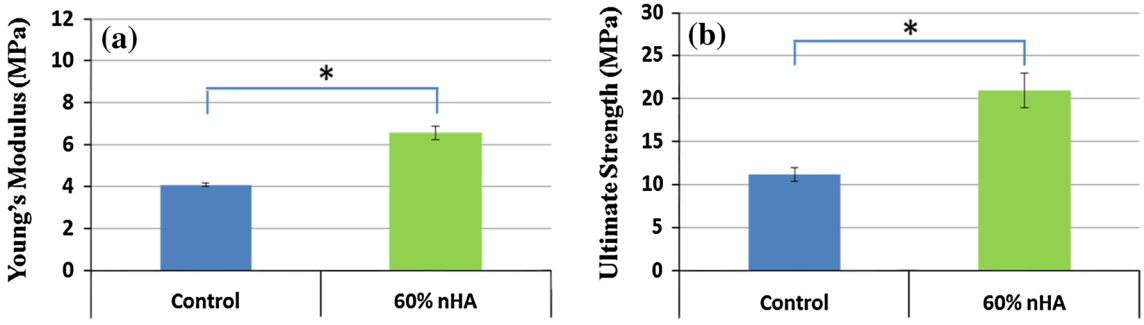

FIGURE 5. Compressive mechanical properties of biphasic osteochondral scaffolds with and without nHA. 60 wt% nHA can greatly improve compressive young's modulus (a) and ultimate compressive strength (b) of fabricated scaffolds. Data are mean ± standard error of the mean, $n = 5$, $^*p < 0.05$ when compared to control without nHA.

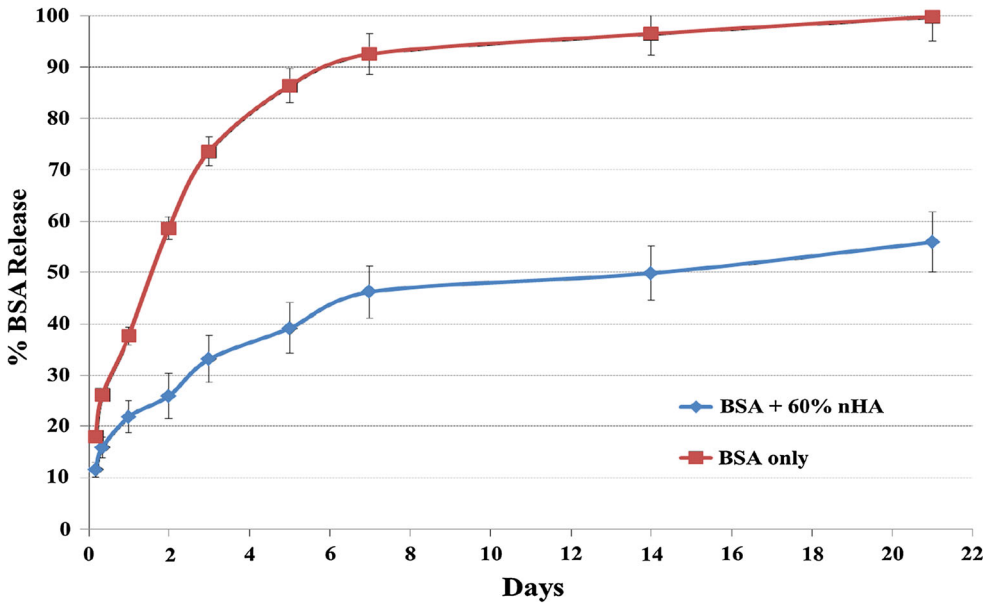

FIGURE 6. Cumulative release kinetics of bioactive BSA encapsulated biphasic osteochondral scaffolds with and without nHA. The nHA scaffold can greatly improve sustained delivery of bioactive BSA over 21 days. Data are mean ± standard error of the mean, $n = 5$.

respectively. Seeded samples were evaluated for GAG, type II collagen, calcium deposition, type I collagen, and total collagen synthesis after 3 weeks of culture.

Specifically, GAG, an important biochemical marker for hMSC chondrogenic differentiation showed increased production upon scaffolds with incorporated nHA and TGF-β1 (Fig. 9). There was a significant increase in GAG content on scaffolds with 60 wt% nHA and TGF-β1 after all time points when compared to control. An increase of 15% over control after 3 weeks of culture was observed on TGF-β1 and nHA-containing scaffolds. In addition, Fig. 10 illustrates another important cartilage matrix protein—type II collagen synthesis upon the biomimetic bioactive nanoosteochondral scaffolds. As a late-stage marker of chondrogenic differentiation, type II collagen synthesis was significantly increased after each time point for all biomimetic biphasic scaffolds when compared to control. All of these data reveal the great potential of this novel scaffold fabrication technique for efficient delivery of TGF-β1 and subsequent improved chondrogenic differentiation of hMSCs. After 1 week of culture, a ~10% increase in type II collagen was observed on all sample groups over control. Even greater type II collagen synthesis was observed after 2 and 3 weeks with an increase of 13 and 33% and 32 and 26% for 60 wt% nHA and 60 wt% nHA with TGF-β1, respectively.

In addition to improved chondrogenic differentiation within our designed osteochondral scaffolds, our nanocomposite osteochondral scaffold with nHA and TGF-β1 is also promising for enhanced osteogenic

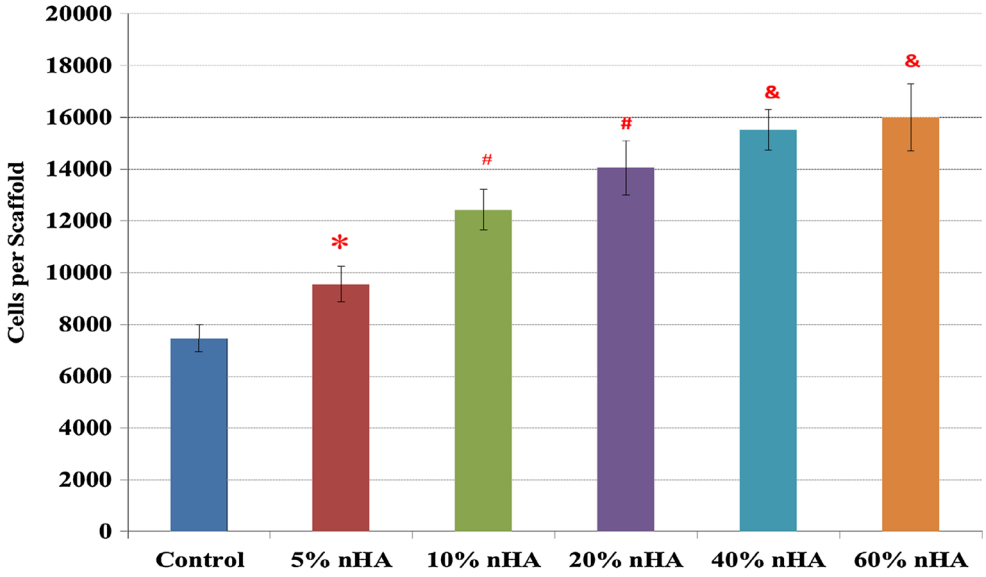

FIGURE 7. Greatly enhanced hMSC adhesion on 3D printed nHA encapsulated osteochondral scaffolds with increasing nHA concentration. Data are mean ± standard error of the mean, $N = 3$, $^{*}p < 0.05$ when compared to control without nHA. $^{\#}p < 0.05$ when compared to control and 5% nHA in the scaffold; and $^{\&}p < 0.05$ when compared to control, 5 and 10% nHA in the scaffold.

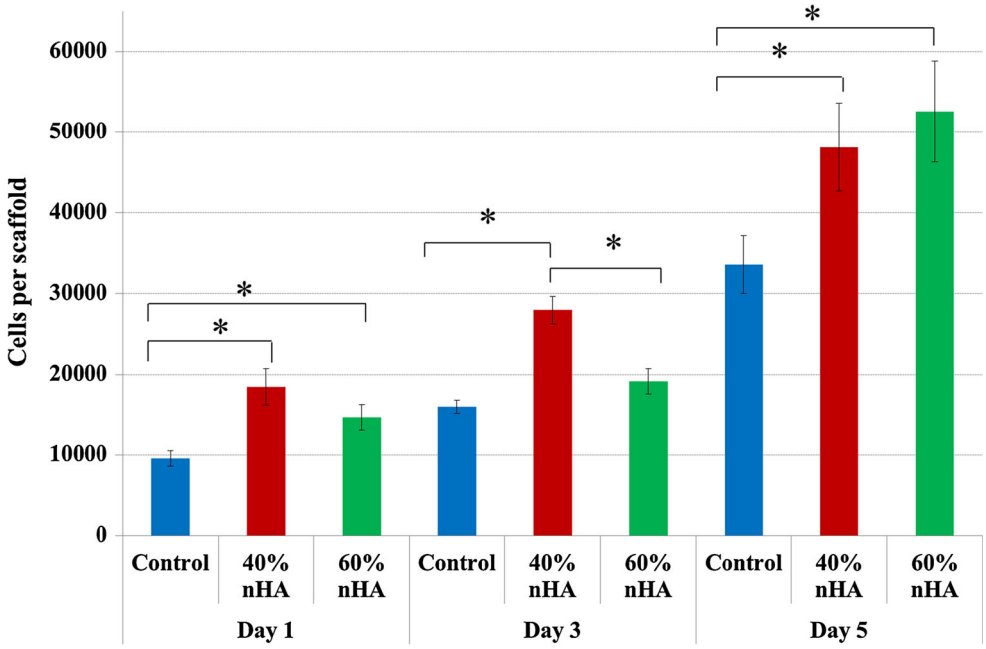

FIGURE 8. hMSC 5-day proliferation study. nHA-containing osteochondral scaffolds exhibited greater proliferative capacity when compared to control after 1, 3, and 5 days, respectively. Data are mean ± standard error of the mean, $N = 3$, $^{*}p < 0.05$.

differentiation of hMSCs. In particular, deposited extracellular calcium results (Fig. 11) revealed greater calcium deposition in all nanocomposite samples after 1 and 2 weeks. Through the incorporation of nHA particles, the results illustrate the effectiveness of nHA induction of early hMSC osteogenesis when compared to control. Both nHA and nHA + TGF-β1 containing nanocomposite scaffolds exhibited increased extracellular calcium deposition of 29 and 24% and 24 and 38% after 1 and 2 weeks culture, respectively, when compared to control. This may be attributed to inhibition of phosphate-induced osteogenesis by TGF-β1 as reported by Guerrero *et al.*[18]

As one of the important extracellular matrix proteins in subchondral bone, type I collagen synthesis was also evaluated (Fig. 12). Although no statistical difference

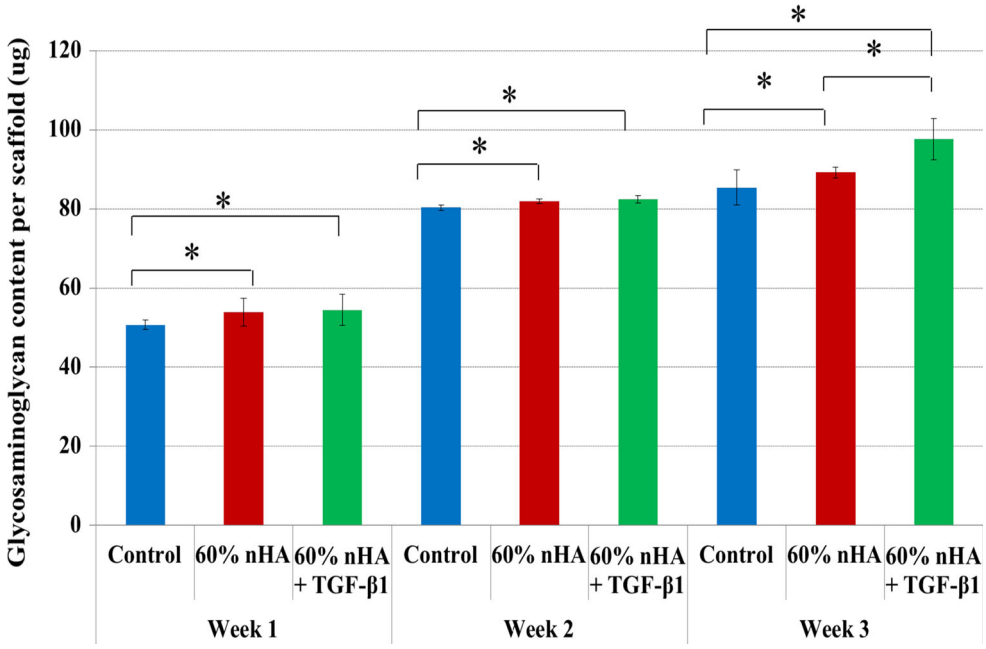

FIGURE 9. Greatly enhanced GAG synthesis on 3D printed osteochondral scaffolds with 60 wt% nHA and TGF-β1 after 1, 2, and 3 weeks when compared to control. Data are mean ± standard error of the mean, $N = 3$, $^*p < 0.05$.

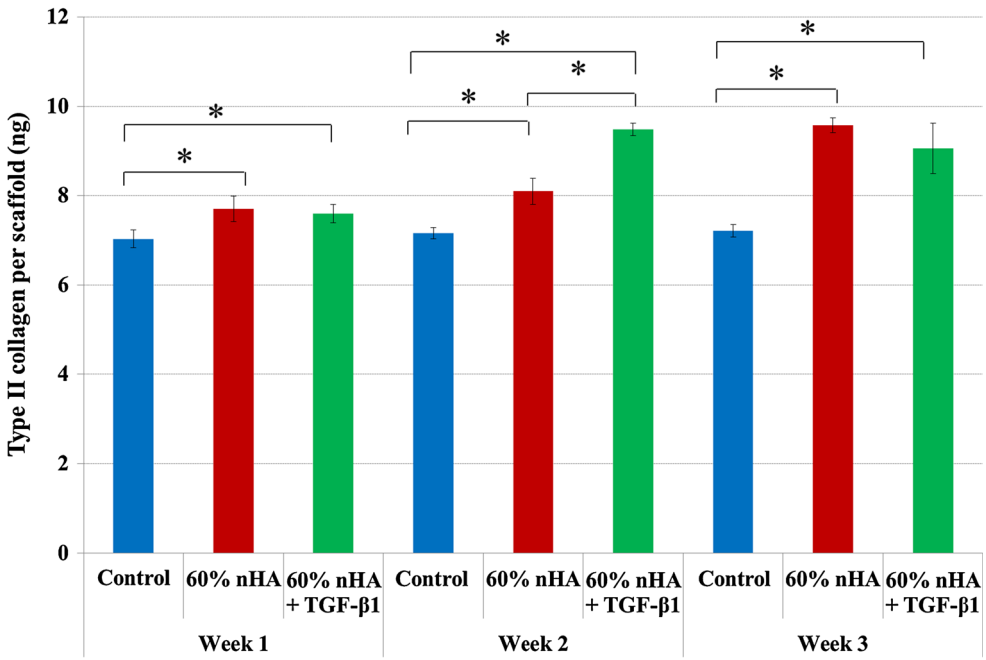

FIGURE 10. Both, TGF-β1 and 60 wt% nHA-containing 3D printed osteochondral scaffolds promoted type II collagen production after 1, 2, and 3 weeks when compared to control. Data are mean ± standard error of the mean, $N = 3$, $^*p < 0.05$.

was observed amongst the experimental and control groups within the first 2 weeks of culture, it was noted that nHA and nHA + TGF-β1 containing osteochondral scaffolds showed increased type I collagen synthesis when compared to control after 3 weeks (116 and 163%) which aids in the promotion of subchondral bone tissue formation. Taken collectively with the observed increase in deposited extracellular calcium, the bioactive nanocomposite scaffold developed herein shows effective induction of hMSC osteogenesis.

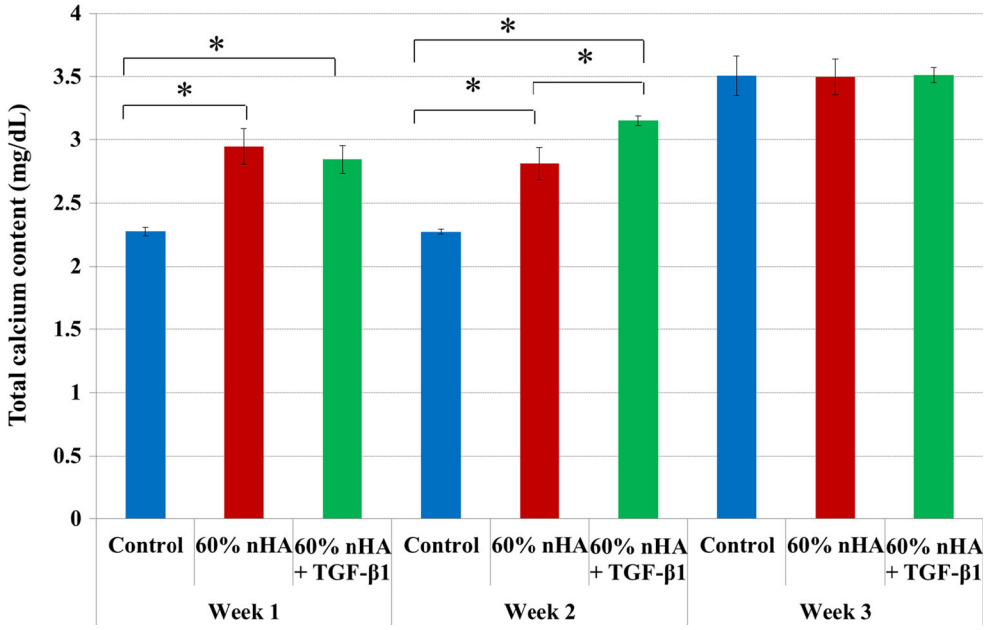

FIGURE 11. nHA containing 3D printed osteochondral scaffolds exhibited increased calcium production when compared to control after 1 and 2 weeks. 60 wt% nHA + TGF-β1 scaffolds displayed greater calcium deposition after 2 weeks when compared to all other groups. Data are mean ± standard error of the mean, $N = 3$, $^*p < 0.05$.

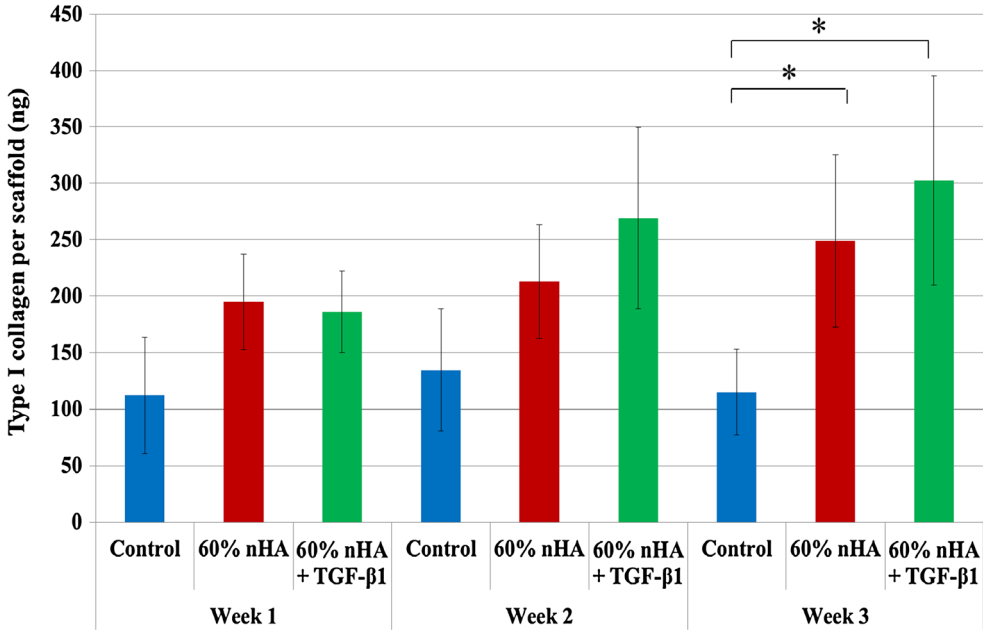

FIGURE 12. Type I collagen synthesis on 3D printed osteochondral scaffolds. 60 wt% nHA + TGF-β1 scaffolds displayed greater type I collagen after 3 weeks when compared to control. Data are mean ± standard error of the mean, $N = 3$, $^*p < 0.05$.

Total collagen synthesis (Fig. 13), a late-stage marker of extracellular matrix formation, increased in nHA and nHA + TGF-β1 bioactive scaffolds with respect to control after 1 week of culture (26 and 78%). The nHA with incorporated TGF-β1 samples achieved the highest rate of collagen synthesis when compared to non-growth factor containing samples after 1 week. In addition, nHA + TGF-β1 scaffolds showed a 30% increase in total collagen production when compared to control after 2 weeks. There was no distinguishable difference observed amongst the groups after 3 weeks.

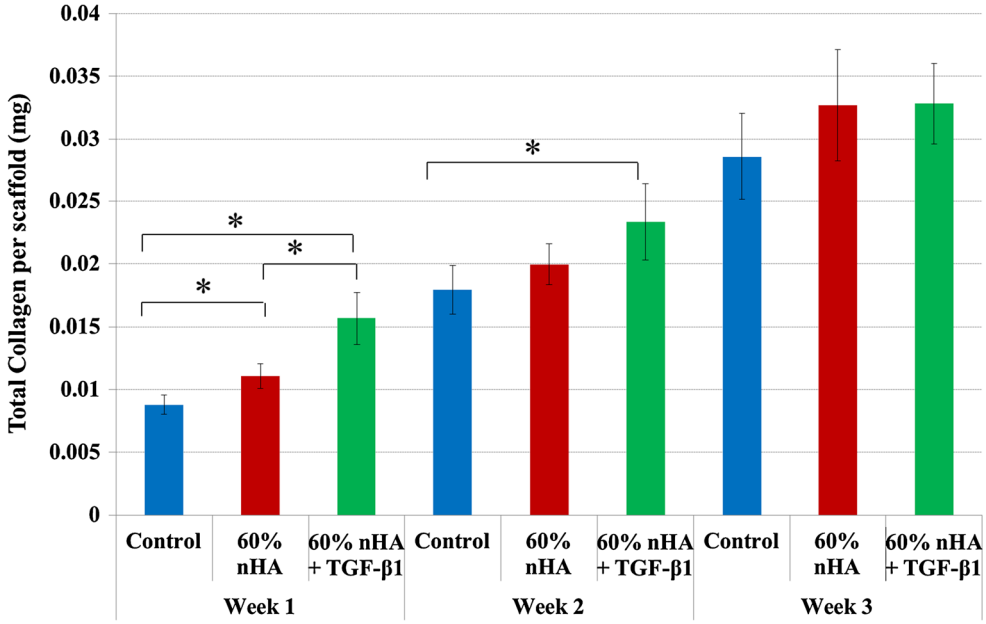

FIGURE 13. nHA and TGF-β1 containing scaffolds displayed enhanced total collagen production after 1 and 2 weeks when compared to control. Data are mean ± standard error of the mean, $N = 3$, $^*p < 0.05$.

DISCUSSION

Investment Casting Based 3D Printing for the Fabrication of Novel Osteochondral Nanocomposite Scaffolds with Suitable Mechanical Properties and Sustained Bioactive Factor Delivery

The current technique of indirect 3D printed nanocomposite scaffold fabrication allows for efficient and effective incorporation of bioactive nanomaterials leading to increased nanoscale surface roughness while retaining the bulk geometry of the predesigned structure. In addition, modifications to the 3D printed sacrificial mold can be readily made where each respective layer's in-fill density (corresponding to pore density of the fabricated scaffold), extruded filament size (pore size of the fabricated hydrogel scaffold), and orientation can be readily controlled creating a gradual transition of porosity and pore geometry. As illustrated through the current work, the composition of the resultant scaffold can be customized to regenerate a particular tissue type through the incorporation of tissue-specific organic and inorganic components in a highly reproducible manner.

In this study, the bulk matrix of the scaffold was also employed as a sustained delivery device which promoted synergistic interactions between the incorporated bioactive factors as evidenced by controlled and sustained bioactive factor delivery. As is known, various growth factors (e.g., TGF-β1 and BMP-2) have been shown to improve MSC osteogenic or chondrogenic differentiation.[2,11,13,17,24,29–32,42,47] However, methods for sustained growth factor delivery face ongoing issues with regards to short-term retention, quick half-life in circulation, and quick loss of biological activity even when administered at high dose rates. When local delivery to the osteochondral defect site is employed, rapid diffusion to adjacent tissues and loss of bioactivity limits their potential to promote prolonged osteochondral tissue formation in the defect site. Therefore, we extended the application of the scaffold design to not only serve as a 3D structural support for cellular attachment, but as a bioactive factor delivery device for sustained release of TGF-β1 in a controlled fashion, thus facilitating long-term osteochondral tissue regeneration. A significant sustained protein release was observed and is postulated to be attributed to electrostatic interactions between the negative carboxyl terminals of the globular protein and positively-charged species (H^+ and Ca^{2+}) of the nHA particles[15] present at the material's surface as described by Tarafder *et al.*[52] as well as electrostatic interactions of the bulk hydrogel matrix. In addition, increased surface roughness and surface area allow for greater protein adsorption and inhibited diffusion, thus extending the localized presence of bioactive factors.

In addition, the capacity of 3D printed scaffolds to withstand compressive loads is important due to the fact that human osteochondral tissue within articulating joints is under repetitive compression during daily activities. Tissue degeneration typically emanates from injury to the cartilage layer which is exacerbated by

mismatches in implant–host tissue stiffness. The scaffolds fabricated here display compressive strength similar to that of native osteochondral tissue and other reported biphasic systems thus rendering the fabricated scaffold less likely to fail.[60] In particular, our hydrothermally treated nHA serves as an excellent mechanical reinforcer within our 3D printed osteochondral construct.

Enhanced hMSC Functions and Osteochondral Matrix Development upon the 3D Printed Nanocomposite Scaffolds

Surface roughness and topography are important features when designing scaffolds for tissue engineering applications.[45] The 3D bioactive nanocomposite scaffold developed here integrated bioactive inorganic ceramics and growth factor delivery in combination with a highly reproducible investment casting method. Scaffolds with interconnected microchannels of approximately 200 μm were created which facilitated cell adhesion, proliferation, and cellular activities. The porous structure allowed for efficient exchange of nutrients and metabolic waste removal during new tissue formation. Through the incorporation of near physiological concentrations of osteoconductive nHA, hMSC adhesion and proliferation were greatly enhanced. nHA is the bioactive and osteoconductive chemical component in bone and the calcified zone in cartilage.[61,63,64] Hydroxyapatite and its derivatives have been studied and shown to increase cell-scaffold performance via incorporation within a bulk matrix as well as surface adsorption[36,37,40] and nucleation.[28,49,58] Through a hydrothermal treatment method, our lab can synthesize more biomimetic nHA with excellent control of the crystalline phase and surface morphology at the nanoscale. Our cell study confirmed that the synthesized nHA can be an excellent osteoconductive chemical cue for improving hMSC adhesion, proliferation and early osteogenesis *in vitro*.

The increase in GAG synthesis on TGF-β1 samples may be attributed to sustained release and synergistic interactions of growth factor and nHA particles as illustrated by the release kinetics. Organic TGF-β1 has been shown to direct early and late-stage MSC chondrogenic and osteogenic differentiation[5] from expedited proliferation to increased GAG production and hypertrophic maturation of seeded MSCs. Tezcan *et al.*[53] examined TGF-β1 induced MSC chondrogenic differentiation and correlated their findings as a dose-dependent response wherein TGF-β1 was critical in the initiation of GAG synthesis and late-stage tissue maturation. Although TGF-β1 was added only to the top cartilage layer, localized diffusion through the entire construct is facilitated by the inherent microporous nature of the PEG-DA hydrogel whose composition consisted of a 40% soluble fraction as characterized in our previous work.[8]

The future clinical applicability of the system developed here has large potential for orthopedic applications. Based on CAD models reconstructed from MRI images of osteochondral tissue defects, a patient-specific nanocomposite osteochondral construct with biomimetic macro architecture can be readily 3D printed to promote better host–implant integration within the defect site and expedite tissue regeneration. Furthermore, not limited to osteochondral regeneration, due to the flexibility of designing 3D structures with varied bioactive composition, the technique developed here can be used to create a variety of other complex tissue constructs via integration different nanobiomaterials and growth factors with biomimetic 3D tissue matrix.

CONCLUSIONS

The work presented here served to illustrate the feasibility of manufacturing a novel biphasic osteochondral nanocomposite scaffold with predesigned nanocomponents to microarchitecture and controlled bioactive factor release. Novel aspects of the current study include the development of an efficient investment casting technique and nanobiomaterials to manufacture novel biphasic and highly interconnected nanoosteochondral scaffolds with sustained and controlled bioactive factor delivery. hMSC adhesion and osteochondral differentiation were greatly enhanced through the incorporation of tissue-specific nHA and TGF-β1. Moreover, due to the flexible design nature of our printing system and CAD modeling, a variety of complex tissue or even organ scaffolds with nanomaterials and growth factors can be realized, thus make them promising for diverse tissue and organ regeneration applications.

ACKNOWLEDGMENTS

The authors would like to thank NIH Director's New Innovator Award (DP2EB020549) and GW Institute for Biomedical Engineering for financial support.

CONFLICT OF INTEREST

Nathan J. Castro, Romil Patel and Lijie Grace Zhang declare that they have no conflicts of interest.

ETHICAL STANDARDS

No human or animal studies were carried out by the authors for this article.

REFERENCES

[1]Akagi, T., T. Fujiwara, and M. Akashi. Inkjet printing of layer-by-layer assembled poly(lactide) stereocomplex with encapsulated proteins. *Langmuir* 30:1669–1676, 2014.

[2]Bai, X., G. Li, C. Zhao, H. Duan, and F. Qu. BMP7 induces the differentiation of bone marrow-derived mesenchymal cells into chondrocytes. *Med. Biol. Eng. Comput.* 49:687–692, 2011.

[3]Bian, W. G., D. C. Li, Q. Lian, X. Li, W. J. Zhang, K. Z. Wang, and Z. M. Jin. Fabrication of a bio-inspired beta-tricalcium phosphate/collagen scaffold based on ceramic stereolithography and gel casting for osteochondral tissue engineering. *Rapid Prototyp. J.* 18:68–80, 2012.

[4]Brady, M. A., S. D. Waldman, and C. R. Ethier. The application of multiple biophysical cues to engineer functional neo-cartilage for treatment of osteoarthritis (Part II: Signal transduction). *Tissue Eng. B* 21(1):20–33, 2015.

[5]Breen, E. C., R. A. Ignotz, L. McCabe, J. L. Stein, G. S. Stein, and J. B. Lian. TGF beta alters growth and differentiation related gene expression in proliferating osteoblasts in vitro, preventing development of the mature bone phenotype. *J. Cell. Physiol.* 160:323–335, 1994.

[6]Cao, T., K. H. Ho, and S. H. Teoh. Scaffold design and in vitro study of osteochondral coculture in a three-dimensional porous polycaprolactone scaffold fabricated by fused deposition modeling. *Tissue Eng.* 9(Suppl 1):S103–S112, 2003.

[7]Castro, N., S. Hacking, and L. Zhang. Recent progress in interfacial tissue engineering approaches for osteochondral defects. *Ann. Biomed. Eng.* 40:1628–1640, 2012.

[8]Castro, N. J., C. M. O'Brien, and L. G. Zhang. Biomimetic biphasic 3-D nanocomposite scaffold for osteochondral regeneration. *AIChE J.* 60:432–442, 2014.

[9]Childs, A., U. D. Hemraz, N. J. Castro, H. Fenniri, and L. G. Zhang. Novel biologically-inspired rosette nanotube PLLA scaffolds for improving human mesenchymal stem cell chondrogenic differentiation. *Biomed. Mater.* 8:065003, 2013.

[10]Chim, H., E. Miller, C. Gliniak, and E. Alsberg. Stromal-cell-derived factor (SDF) 1-alpha in combination with BMP-2 and TGF-beta1 induces site-directed cell homing and osteogenic and chondrogenic differentiation for tissue engineering without the requirement for cell seeding. *Cell Tissue Res.* 350:89–94, 2012.

[11]Chim, H., E. Miller, C. Gliniak, and E. Alsberg. Stromal-cell-derived factor (SDF) 1-alpha in combination with BMP-2 and TGF-beta1 induces site-directed cell homing and osteogenic and chondrogenic differentiation for tissue engineering without the requirement for cell seeding. *Cell Tissue Res.* 350:89–94, 2012.

[12]Chua, C. K., K. F. Leong, N. Sudarmadji, M. J. J. Liu, and S. M. Chou. Selective laser sintering of functionally graded tissue scaffolds. *MRS Bull.* 36:1006–1014, 2011.

[13]Davis, H. E., E. M. Case, S. L. Miller, D. C. Genetos, and J. K. Leach. Osteogenic response to BMP-2 of hMSCs grown on apatite-coated scaffolds. *Biotechnol. Bioeng.* 108:2727–2735, 2011.

[14]Dormer, N. H., K. Busaidy, C. J. Berkland, and M. S. Detamore. Osteochondral interface regeneration of the rabbit mandibular condyle with bioactive signal gradients. *J. Oral Maxillofac. Surg.* 69:e50–e57, 2011.

[15]Embery, G., G. Rolla, and J. B. Stanbury. Interaction of acid glycosaminoglycans (mucopolysaccharides) with hydroxyapatite. *Scand. J. Dent. Res.* 87:318–324, 1979.

[16]Enea, D., S. Cecconi, S. Calcagno, A. Busilacchi, S. Manzotti, C. Kaps, and A. Gigante. Single-stage cartilage repair in the knee with microfracture covered with a resorbable polymer-based matrix and autologous bone marrow concentrate. *Knee* 20:562–569, 2013.

[17]Ertan, A. B., P. Yilgor, B. Bayyurt, A. C. Calikoglu, C. Kaspar, F. N. Kok, G. T. Kose, and V. Hasirci. Effect of double growth factor release on cartilage tissue engineering. *J. Tissue Eng. Regen. Med.* 7:149–160, 2013.

[18]Guerrero, F., C. Herencia, Y. Almaden, J. M. Martinez-Moreno, A. Montesdeoca, M. E. Rodriguez-Ortiz, J. M. Diaz-Tocados, A. Canalejo, M. Florio, I. Lopez, W. G. Richards, M. Rodriguez, E. Aguilera-Tejero, and J. R. Munoz-Castaneda. TGF-beta prevents phosphate-induced osteogenesis through inhibition of BMP and Wnt/beta-catenin pathways. *PLoS ONE* 9:e89179, 2014.

[19]Holmes, B., N. J. Castro, J. Li, M. Keidar, and L. G. Zhang. Enhanced human bone marrow mesenchymal stem cell functions in novel 3D cartilage scaffolds with hydrogen treated multi-walled carbon nanotubes. *Nanotechnology* 24:365102, 2013.

[20]Holmes, B., A. Zarate, M. Keidar, and L. G. Zhang. Enhanced human bone marrow mesenchymal stem cell chondrogenic differentiation in electrospun constructs with carbon nanomaterials. *Carbon* 97:1–13, 2016.

[21]Holmes, B., W. Zhu, J. Li, J. D. Lee, and L. G. Zhang. Development of novel 3D printed scaffolds for osteochondral regeneration. *Tissue Eng. A* 21:403–415, 2015.

[22]Holzapfel, B. M., J. C. Reichert, J. T. Schantz, U. Gbureck, L. Rackwitz, U. Noth, F. Jakob, M. Rudert, J. Groll, and D. W. Hutmacher. How smart do biomaterials need to be? A translational science and clinical point of view. *Adv. Drug Deliv. Rev.* 65:581–603, 2013.

[23]Hootman, J. M., and C. G. Helmick. Projections of US prevalence of arthritis and associated activity limitations. *Arthritis Rheum.* 54:226–229, 2006.

[24]Huang, W. B., B. Carlsen, I. Wulur, G. Rudkin, K. Ishida, B. Wu, D. T. Yamaguchi, and T. A. Miller. BMP-2 exerts differential effects on differentiation of rabbit bone marrow stromal cells grown in two-dimensional and three-dimensional systems and is required for in vitro bone formation in a PLGA scaffold. *Exp. Cell Res.* 299:325–334, 2004.

[25]Hutmacher, D. W., and S. Cool. Concepts of scaffold-based tissue engineering-the rationale to use solid free-form fabrication techniques. *J. Cell Mol. Med.* 11:654–669, 2007.

[26]Hutmacher, D. W., M. Sittinger, and M. V. Risbud. Scaffold-based tissue engineering: rationale for computer-aided design and solid free-form fabrication systems. *Trends Biotechnol.* 22:354–362, 2004.

[27]Im, O., J. Li, M. Wang, L. G. Zhang, and M. Keidar. Biomimetic three-dimensional nanocrystalline hydroxyapatite and magnetically synthesized single-walled carbon nanotube chitosan nanocomposite for bone regeneration. *Int. J. Nanomedicine* 7:2087–2099, 2012.

[28]Iwatsubo, T., K. Sumaru, T. Kanamori, T. Shinbo, and T. Yamaguchi. Construction of a new artificial biomineralization system. *Biomacromolecules* 7:95–100, 2006.

[29]Kim, M., I. E. Erickson, M. Choudhury, N. Pleshko, and R. L. Mauck. Transient exposure to TGF-beta3 improves

the functional chondrogenesis of MSC-laden hyaluronic acid hydrogels. *J. Mech. Behav. Biomed. Mater.* 11:92–101, 2012.
[30]Kim, J., I. S. Kim, T. H. Cho, K. B. Lee, S. J. Hwang, G. Tae, I. Noh, S. H. Lee, Y. Park, and K. Sun. Bone regeneration using hyaluronic acid-based hydrogel with bone morphogenic protein-2 and human mesenchymal stem cells. *Biomaterials* 28:1830–1837, 2007.
[31]Kim, S. E., H. K. Rha, S. Surendran, C. W. Han, S. C. Lee, H. W. Choi, Y. W. Choi, K. H. Lee, J. W. Rhie, and S. T. Ahn. Bone morphogenic protein-2 (BMP-2) immobilized biodegradable scaffolds for bone tissue engineering. *Macromol. Res.* 14:565–572, 2006.
[32]Kwon, S. H., T. J. Lee, J. Park, J. E. Hwang, M. Jin, H. K. Jang, N. S. Hwang, and B. S. Kim. Modulation of BMP-2-induced chondrogenic versus osteogenic differentiation of human mesenchymal stem cells by cell-specific extracellular matrices. *Tissue Eng. A* 19:49–58, 2013.
[33]Lee, J. Y., B. Choi, B. Wu, and M. Lee. Customized biomimetic scaffolds created by indirect three-dimensional printing for tissue engineering. *Biofabrication* 5:045003, 2013.
[34]Lee, S. J., H. W. Kang, J. K. Park, J. W. Rhie, S. K. Hahn, and D. W. Cho. Application of microstereolithography in the development of three-dimensional cartilage regeneration scaffolds. *Biomed. Microdevices* 10:233–241, 2008.
[35]Liu, T., G. Wu, Y. Zheng, D. Wismeijer, V. Everts, and Y. Liu. Cell-mediated BMP-2 release from a novel dual-drug delivery system promotes bone formation. *Clin Oral Implants Res.* 25:1412–1421, 2014.
[36]Madhumathi, K., K. T. Shalumon, V. V. Rani, H. Tamura, T. Furuike, N. Selvamurugan, S. V. Nair, and R. Jayakumar. Wet chemical synthesis of chitosan hydrogel-hydroxyapatite composite membranes for tissue engineering applications. *Int. J. Biol. Macromol.* 45:12–15, 2009.
[37]Matsumura, K., T. Hayami, S. H. Hyon, and S. Tsutsumi. Control of proliferation and differentiation of osteoblasts on apatite-coated poly(vinyl alcohol) hydrogel as an artificial articular cartilage material. *J. Biomed. Mater. Res. A* 92:1225–1232, 2010.
[38]Melchels, F. P. W., M. A. N. Domingos, T. J. Klein, J. Malda, P. J. Bartolo, and D. W. Hutmacher. Additive manufacturing of tissues and organs. *Prog. Polym. Sci.* 37:1079–1104, 2012.
[39]Miller, J. S., K. R. Stevens, M. T. Yang, B. M. Baker, D.-H. T. Nguyen, D. M. Cohen, E. Toro, A. A. Chen, P. A. Galie, X. Yu, R. Chaturvedi, S. N. Bhatia, and C. S. Chen. Rapid casting of patterned vascular networks for perfusable engineered three-dimensional tissues. *Nat. Mater.* 11:768–774, 2012.
[40]Moreau, D., A. Villain, D. N. Ku, and L. Corte. Poly(vinyl alcohol) hydrogel coatings with tunable surface exposure of hydroxyapatite. *Biomatter* 4:e28764, 2014.
[41]Ng, K. W., P. A. Torzilli, R. F. Warren, and S. A. Maher. Characterization of a macroporous polyvinyl alcohol scaffold for the repair of focal articular cartilage defects. *J. Tissue Eng. Regen. Med.* 8:164–168, 2014.
[42]Noel, D., D. Gazit, C. Bouquet, F. Apparailly, C. Bony, P. Plence, V. Millet, G. Turgeman, M. Perricaudet, J. Sany, and C. Jorgensen. Short-term BMP-2 expression is sufficient for in vivo osteochondral differentiation of mesenchymal stem cells. *Stem Cells* 22:74–85, 2004.
[43]O'Brien, C., B. Holmes, S. Faucett, and L. G. Zhang. 3D printing of nanomaterial scaffolds for complex tissue regeneration. *Tissue Eng. B* 21:103–114, 2015.
[44]Park, S., G. Kim, Y. C. Jeon, Y. Koh, and W. Kim. 3D polycaprolactone scaffolds with controlled pore structure using a rapid prototyping system. *J. Mater. Sci. Mater. Med.* 20:229–234, 2009.
[45]Place, E. S., J. H. George, C. K. Williams, and M. M. Stevens. Synthetic polymer scaffolds for tissue engineering. *Chem. Soc. Rev.* 38:1139–1151, 2009.
[46]Schumann, D., A. K. Ekaputra, C. X. Lam, and D. W. Hutmacher. Biomaterials/scaffolds. Design of bioactive, multiphasic PCL/collagen type I and type II-PCL-TCP/collagen composite scaffolds for functional tissue engineering of osteochondral repair tissue by using electrospinning and FDM techniques. *Methods Mol. Med.* 140:101–124, 2007.
[47]Sekiya, I., D. C. Colter, and D. J. Prockop. BMP-6 enhances chondrogenesis in a subpopulation of human marrow stromal cells. *Biochem. Biophys. Res. Commun.* 284:411–418, 2001.
[48]Serra, T., J. A. Planell, and M. Navarro. High-resolution PLA-based composite scaffolds via 3-D printing technology. *Acta Biomater.* 9:5521–5530, 2013.
[49]Sugino, A., T. Miyazaki, and C. Ohtsuki. Apatite-forming ability of polyglutamic acid hydrogels in a body-simulating environment. *J. Mater. Sci. Mater. Med.* 19:2269–2274, 2008.
[50]Sun, L., L. Zhang, U. D. Hemraz, H. Fenniri, and T. J. Webster. Bioactive rosette nanotube-hydroxyapatite nanocomposites improve osteoblast functions. *Tissue Eng. A* 18:1741–1750, 2012.
[51]Swieszkowski, W., B. H. Tuan, K. J. Kurzydlowski, and D. W. Hutmacher. Repair and regeneration of osteochondral defects in the articular joints. *Biomol. Eng.* 24:489–495, 2007.
[52]Tarafder, S., S. Banerjee, A. Bandyopadhyay, and S. Bose. Electrically polarized biphasic calcium phosphates: adsorption and release of bovine serum albumin. *Langmuir* 26:16625–16629, 2010.
[53]Tezcan, B., S. Serter, E. Kiter, and A. C. Tufan. Dose dependent effect of C-type natriuretic peptide signaling in glycosaminoglycan synthesis during TGF-beta1 induced chondrogenic differentiation of mesenchymal stem cells. *J. Mol. Histol.* 41:247–258, 2010.
[54]Walther, M., S. Altenberger, S. Kriegelstein, C. Volkering, and A. Roser. Reconstruction of focal cartilage defects in the talus with miniarthrotomy and collagen matrix. *Oper. Orthop. Traumatol.* 26:603–610, 2014.
[55]Wang, M., N. J. Castro, J. Li, M. Keidar, and L. G. Zhang. Greater osteoblast and mesenchymal stem cell adhesion and proliferation on titanium with hydrothermally treated nanocrystalline hydroxyapatite/magnetically treated carbon nanotubes. *J. Nanosci. Nanotechnol.* 12:7692–7702, 2012.
[56]Wang, M., X. Cheng, W. Zhu, B. Holmes, M. Keidar, and L. G. Zhang. Design of biomimetic and bioactive cold plasma-modified nanostructured scaffolds for enhanced osteogenic differentiation of bone marrow-derived mesenchymal stem cells. *Tissue Eng. A.* 20:1060–1071, 2013.
[57]Wu, M., H. Dong, K. Guo, R. Zeng, M. Tu, and J. Zhao. Self-assemblied nanocomplexes based on biomimetic amphiphilic chitosan derivatives for protein delivery. *Carbohydr. Polym.* 121:115–121, 2015.
[58]Wu, L. C., J. Yang, and J. Kopecek. Hybrid hydrogels self-assembled from graft copolymers containing complementary beta-sheets as hydroxyapatite nucleation scaffolds. *Biomaterials* 32:5341–5353, 2011.

[59]Zhang, L., Y. Chen, J. Rodriguez, H. Fenniri, and T. J. Webster. Biomimetic helical rosette nanotubes and nanocrystalline hydroxyapatite coatings on titanium for improving orthopedic implants. *Int. J. Nanomedicine* 3:323–333, 2008.
[60]Zhang, L., J. Hu, and K. A. Athanasiou. The role of tissue engineering in articular cartilage repair and regeneration. *Crit. Rev. Biomed. Eng*. 37:1–57, 2009.
[61]Zhang, L., J. Y. Li, and J. D. Lee. Nanocomposites for cartilage regeneration. In: Nanomedicine: technologies and applications, edited by T. J. Webster. Cambridge: Woodhead Publishing Limited, 2012, pp. 571–598.
[62]Zhang, L., J. Rodriguez, J. Raez, A. J. Myles, H. Fenniri, and T. J. Webster. Biologically inspired rosette nanotubes and nanocrystalline hydroxyapatite hydrogel nanocomposites as improved bone substitutes. *Nanotechnology* 20:175101, 2009.
[63]Zhang, L., S. Sirivisoot, G. Balasundaram, and T. J. Webster. Nanomaterials for improved orthopedic and bone tissue engineering applications. In: Advanced biomaterials: fundamentals, processing and application, edited by B. Basu, D. Katti, and A. Kuma. New York: Wiley, 2009, pp. 205–241.
[64]Zhang, L., and T. J. Webster. Nanotechnology and nanomaterials: promises for improved tissue regeneration. *Nanotoday* 4:66–80, 2009.
[65]Zhu, W., M. Wang, Y. Fu, N. J. Castro, S. W. Fu, and L. G. Zhang. Engineering a biomimetic three-dimensional nanostructured bone model for breast cancer bone metastasis study. *Acta Biomater*. 14:164–174, 2015.